



OPEN

Liquid crystal self-templating approach to ultrastrong and tough biomimetic composites

SUBJECT AREAS:

LIQUID CRYSTALS

SELF-ASSEMBLY

MECHANICAL AND STRUCTURAL
PROPERTIES AND DEVICES

MECHANICAL PROPERTIES

Xiaozhen Hu, Zhen Xu, Zheng Liu & Chao Gao

MOE Key Laboratory of Macromolecular Synthesis and Functionalization, Department of Polymer Science and Engineering, Zhejiang University, 38 Zheda Road, Hangzhou 310027, P. R. China.

Received
3 June 2013Accepted
22 July 2013Published
6 August 2013Correspondence and
requests for materials
should be addressed to
C.G. (chaogao@zju.
edu.cn)

Materials with both high strength and toughness are in great demand for a wide range of applications, requiring strict design of ingredients and hierarchically ordered architecture from nano- to macro-scale. Nacre achieves such a target in the long natural evolution by alternative alignment of inorganic nanoplatelets and biomacromolecules. To mimic nacre, various strategies were developed, approaching nacre-comparable performance in limited size. How to remarkably exceed nacre in both property and size is a key issue to further the advancement of composites. Here we present liquid crystal self-templating methodology to make the next generation of ultrastrong and tough nacre-mimics continuously. The hierarchically assembled composites show the highest tensile strength (652 MPa) among nacre mimics, five to eight times as high as that of nacre (80–135 MPa), and excellent ductility with toughness of 18 MJ m⁻³, one to two orders of magnitude greater than that of nacre (0.1 ~ 1.8 MJ m⁻³).

The progress of human life necessitates the incessant development of lightweight, strong and tough materials. Unfortunately, high strength and high toughness are disposed to conflict with each other in the artificial composites¹. To answer this challenge, we can learn from nature, since many natural materials such as nacre and bone are strong and tough due to their hierarchically assembled structures^{2–4}. Consequently, several strategies (e.g., layer-by-layer (LbL) deposition, freezing-drying, and filtration) were proposed to mimic them^{5–17}, especially nacre that possessed ordered brick-and-mortar (B&M) arrangement of inorganic nanoplatelets (~ 95 vol%) and small amount of biomacromolecules^{3,4}. The efforts in the past two decades made nacre-comparable composites available in limited dimension, whereas the mechanical property of such materials was still far from satisfying. Covalent cross-linking could substantially improve the tensile strength (σ) of nacre-mimics (~ 400 MPa) at the sacrifice of ductility (~ 0.3% of strain, ϵ)⁸. The toughness of polymer matrix could be preserved to some extent by incorporation of less amount of nanofillers (≤ 15 vol%), whereas the strength improvement was restricted (σ 315 MPa)¹⁰. Hence, to approach the supreme strength of layered nanocomposites with good ductility simultaneously in large-scale is a big challenge yet.

To address such a fundamental issue, the crucial design is to translate the intrinsic extraordinary property of individual nanoplatelets into highly ordered macroscopic composites by effective assembly. Liquid crystals (LCs) are self-assembled soft materials which possess both the liquid-like mobility and the crystal-like ordering¹⁸. The latter character gives us an opportunity to develop novel materials with nanoparticles aligned in macroscopic scale using LCs as precursors or templates^{19,20}. As a representative successful example, liquid crystalline (LC) carbon nanotubes (CNTs) were utilized to fabricate multifunctional and strong fibres^{21–24}. Graphene, an allotropic substance of CNTs, also exhibits extraordinary thermal, mechanical, and electrical attributes, providing it a fertile ground for many applications²⁵. Recently, LCs of graphene and graphene oxide (GO) have been discovered^{26–28}, and continuous, neat graphene fibres have been achieved consequently^{29–32}. Graphene-based biomimetic composites (e.g., films and fibres) were obtained by either vacuum-assisted filtration assembly or wet-spinning assembly approach^{15–17,33–35}. However, the mechanical performance of these artificial nacre materials ($\sigma \leq 210$ MPa) only approached to that of nacre, still far behind that of theoretical calculation results for graphene-based composites ($\sigma \sim 1.7$ GPa)³⁶, mainly because of numerous defects and weak interfacial interaction between graphene sheets³⁷.

Here we combine liquid crystal self-templating (LCST) approach and wet-spinning technology to continuously fabricate biomimetic composites for the first time. Guest compounds such as polymers and nanoparticles were homogeneously dispersed into the inter-channels of LC GO sheets. The incorporation of wet-spinning



technology gave birth to nacre-mimetic fibres up to thirty meters long with highly ordered hierarchical structure. The integration of ultrahigh aspect ratio and well-preserved alignment of GO sheets, uniform single-molecule interlayer of polymers, and adaptive hydrogen bonding arrays guarantee the macroscopic assembled artificial nacre high σ and toughness (σ 555 MPa, 18 MJ m⁻³), around 2–17 times higher than that of nacre (80–135 MPa, 0.1–1.8 MJ m⁻³)^{2,3}. Due to its lightweight attribute (~ 1.0 g cm⁻³), the highest specific strength of nacre-mimics (652 N m g⁻¹) is around two times that of steel and various alloys such as Mg alloys, Al alloys, and Ti alloys (≤ 300 N m g⁻¹)^{9,11,38}. Moreover, the reduced composites show high electrical conductivity (~ 5261 S m⁻¹), comparable to that of neat graphene papers³⁹.

Results

Synthesis strategy. Wet-spinning of GO LCs gave birth to continuous neat graphene fibres in which graphene sheets aligned regularly along the fibre axis direction²⁹. If strong binder could be introduced into GO LC suspensions, high performance bio-mimetic composites would be available. Accordingly, we present LCST strategy, as shown in Figure 1a–c. To decrease the defects of assembled composites, we firstly synthesized giant graphene oxide (GGO) sheets with average aspect ratio of $\sim 1.6 \times 10^4$ (Supplementary Fig. S1). Such GGO can form lyotropic LCs at a very low concentration (~ 0.5 mg mL⁻¹, Supplementary Fig. S2). To the aqueous solution of GGO LCs, desired guest compounds (e.g., polymers, inorganic nanoparticles) were added. Due to the templating role of GGO LCs, the guest compounds were evenly localized in the interlayer channels of GGO sheets, forming host-guest composite LCs. The LC behaviors of neat GGO and composites were confirmed by polarized optical microscopy (POM) (Fig. 1d,e). Continuous tailor-made biomimetic fibres were fabricated by industrially viable wet-spinning approach (Fig. 1f, Supplementary Fig. S3). Because of the confining effect of GGO sheets to the guests, phase separation between GGO sheets and guests was avoided, and thus uniform B&M structures were well preserved in the resulting solid fibres. The fibres exhibited good flexibility and could be fabricated into a textile by hand (Fig. 1g). Such a LCST strategy has multiple advantages: long-term ordered alignment of GGO sheets originated from LC feature that makes the assembled micro-structure regular even in a large-scale, evenly dispersed guests for the templating of interchannels that results in uniform d -space and thus equal load transfer under tension, generality for accessing multifunctional composites with designed hosts and guests, as well as simple, green, fast, and scalable. Herein, hyperbranched polyglycerol (HPG) was mainly selected as a model

polymer to demonstrate the effectiveness of LCST methodology, as HPG was viscous liquid at room temperature with low mechanical strength.

Wet-spinning assembly process. POM and scanning electron microscopy (SEM) were utilized to trace the wet-spinning process. Figure 2a shows the photograph of spinning dope near the nozzle under crossed polarizers. LC textures were observed in the capillary and at the tip (Fig. 2b,c), indicating that the GGO sheets maintained regular arrangement along with the decrease of nozzle diameter. After injected into the coagulation bath, the ordered alignment was well preserved as gel fibres became thinner and thinner, and finally solid fibres with regularly compact B&M micro-structures were obtained after drying, as demonstrated by *in situ* POM and SEM observations (Fig. 2d–i, Supplementary Fig. S4).

Upon the exchange of solvent and coagulation bath, the fibres contracted in both axial and radial directions. The axial contraction brought crumpled surface that would lead to the decrease of σ . So we stretched the GGO-HPG gel fibres in the coagulation bath by a flowing field (Supplementary Fig. S3). The resultant solid fibres after wet-stretching had unhindered surfaces with spreading ridges along axial direction (Fig. 2j,k). The compressing in radial direction provided GGO-HPG fibres densely aligned, homogeneously layered cross-section structures of alternative GGO sheets and HPG molecules (Fig. 2h,i, Supplementary Fig. S5), implying the absence of phase separation in our bio-mimetic composites with extremely high fraction of nanofillers (69.3–84.2 wt%).

Mechanical properties of GGO-HPG fibres. The hierarchically assembled structures especially the uniform alignment of GGO sheets offer GGO-HPG composite fibres splendid mechanical performance. Figure 3a shows the typical stress-strain profile of fibres. The σ of bio-mimetic fibres is 555 MPa, which is at least 2 times higher than that of nacre mimics made from montmorillonite (MTM) without cross-linking (≤ 170 MPa, Fig. 3b)³, 75% higher than that of Al₂O₃-chitosan composites (315 MPa)¹⁰, 2–4 times σ of GO and graphene-based bio-inspired composites (120–206 MPa)^{15–17,35}, 3 times σ of bone (150 MPa)⁴⁰, and 4 times σ of nacre (135 MPa)⁴¹. Our as-spun composite fibres outstrip the ever strongest, cross-linked nacre-mimics (400 MPa) by about 38% in σ (Table 1)⁸. The σ of GGO-HPG fibres is 60% higher than that of neat GGO fibres (345 MPa), demonstrating the unique binding role of HPG in the composites (Supplementary Fig. S6, S7). FT-IR spectrum of GGO shows several characteristic peaks of various functional groups including O–H (3420 cm⁻¹), C=O (1725 cm⁻¹), and C–O

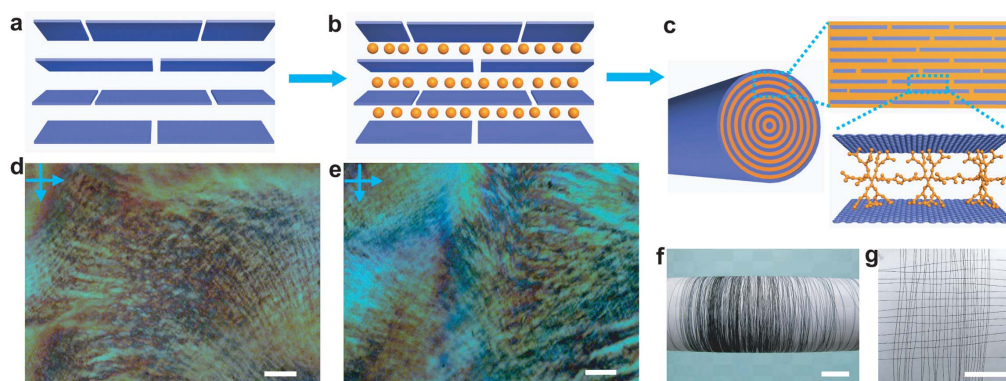


Figure 1 | Schematic illustration of LCST strategy and the resulting composite fibres. (a–c) LCST protocol to prepare host-guest layer-structured composites: formation of host LCs of 2D nanoplatelets with uniform nanochannels (a), incorporation of guest compounds (e.g., polymers, biomacromolecules, and nanoparticles) into the host nanochannels to give host-guest complex LCs (b), and wet-spinning assembly of complex LCs into nacre-mimetic fibres with hierarchical structures (c). (d,e) POM images of host GGO LCs (d) and host-guest complex GGO-HPG LCs (e) loaded in the planar cells with concentration of 4 mg mL⁻¹. (f,g) Photographs of a thirty metres long GGO-HPG fibre (f) and a mat of GGO-HPG fibres made by hand (g). Scale bars, 300 μ m (d,e) and 1 cm (f,g).

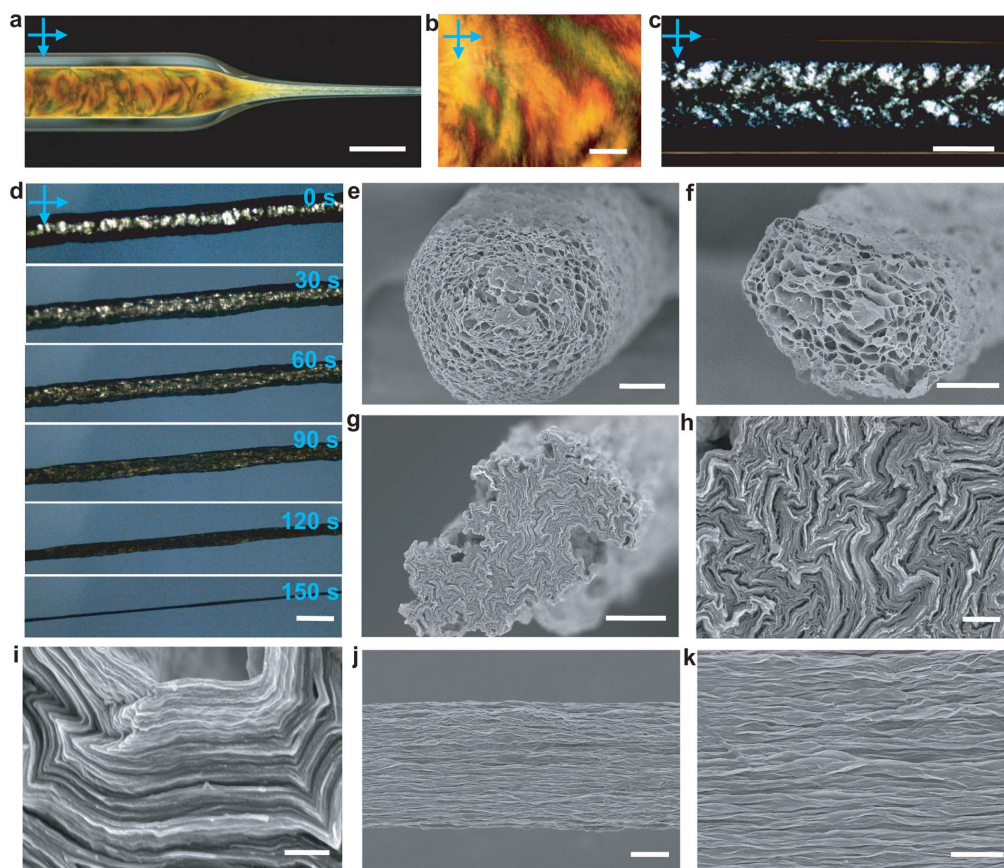


Figure 2 | Structural changes of GGO-HPG during spinning. (a) Photograph of GGO-HPG spinning solution inside the glass spinning head under crossed polarizers. (b–d) POM images of GGO-HPG spinning solution in the capillary (b), at the spinning nozzle (c), and the drying procedure of GGO-HPG fibre (d). (e–k) SEM images of cross-section of a GGO-HPG gel fibre at coagulation time of 0 min (e), 3 min (f), and dried fibre (g–i), the surface morphology of the resulting fibre (j,k). Scale bars, 5 mm (a), 500 μm (b), 250 μm (c), 100 μm (d), 30 μm (e), 25 μm (f), 3 μm (g,k), 500 nm (h), 250 nm (i), and 5 μm (j).

(1045 cm^{-1}), and these abundant groups provide the basis of hydrogen bonding formation. After the introduction of HPG, the wavenumber of O–H shifts to 3400 cm^{-1} , indicating the increase of hydrogen bonding density between HPG and GGO (Supplementary Fig. S6)⁴². Similarly, Buehler and co-workers studied the mechanical properties of neat GO as well as GO/polyvinyl alcohol (PVA) composites in a joint experimental-theoretical and computational study³⁶. Their results not only demonstrated that hydrogen bonding interactions formed in neat GO system, but also proved that hydroxyl groups of PVA and oxygen moieties of GO could form cooperative hydrogen-bonding network, which contributed to the macro-scale mechanical properties of materials. Our multi-hydroxyl HPG, an analogue of PVA, can also form hydrogen bonding network with GGO sheets by analogy.

A better appreciation of the extraordinary mechanical properties of our composites can be accessed via comparison with conventional engineering metallic alloys. Due to the hierarchical ordered architectures at multiple scales and lightweight attribute (density of $\sim 1 \text{ g cm}^{-3}$), our biomimetic composites display much higher specific strength ($\sim 555 \text{ N m g}^{-1}$) than those of engineering materials ($\leq 300 \text{ N m g}^{-1}$), such as Mg alloys, Ti alloys, Al alloys, and steel (Fig. 3c). These results highlight the tremendous potential of our nacre mimics and suggest promising wide range of applications.

The area under the stress-strain curve in Figure 3a provides the volumetric toughness, which is 18 MJ m^{-3} for GGO-HPG nacre-mimic fibre. This value is 4.6 times as high as that of GO-based ultratough artificial nacre (3.91 MJ m^{-3})¹⁷, and one order of magnitude higher than those of pristine GO papers, Ca^{2+} cross-linked

GO papers⁴³, borate cross-linked GO papers³⁵, hydrazine reduced GO papers ($< 2 \text{ MJ m}^{-3}$)³⁹, and our previous biomimetic fibres (1.27 MJ m^{-3}) (Fig. 3b)³³. Other typical artificial nacre composites such as MTM-PVA, MTM-PVA-glutaraldehyde (GA), MTM-chitosan, and MTM-polyelectrolyte also have toughness lower than 2 MJ m^{-3} ,^{8,11,13,14} which is far below that of our composite fibres. Moreover, the toughness of our composites is around 10 times that of natural nacre (1.8 MJ m^{-3})⁴¹, and 15 times that of bone (1.2 MJ m^{-3})⁴⁰. The high toughness of GGO-HPG fibres results from the self-adapting character of supramolecular hydrogen bonding linkages inter- and intra-layers and large aspect ratio of GGO that provides longer slipping distance (Fig. 3d, Supplementary Fig. S6, S1). Additionally, the high toughness may be further enhanced by introducing CNTs into our fibres, utilizing the synergistic effect of graphene and CNTs⁴⁴.

The possible fracture mechanism of GGO-HPG composites is as below: the relatively weak layer of HPG works under small tensile force, as the force increases, it transfers from HPG layer to GGO sheets. Afterwards, GGO sheets and HPG interlayers start to yield in shear and slide on one another, accompanied with the destruction and reformation of the hydrogen bonding networks between the adjacent GGO sheets and HPG interlayers (Fig. 3d). Upon increasing the tensile force, the shear spreads all over the fibres, followed by failure of fibres by pull-out as well as fracture of GGO sheets, as shown in Figure 4a–f and Supplementary Fig. S8. Our SEM observations are in agreement with the theoretical calculation for the layered nanocomposites that predicts fracture of individual nanoplatelets with a high aspect ratio¹⁰.

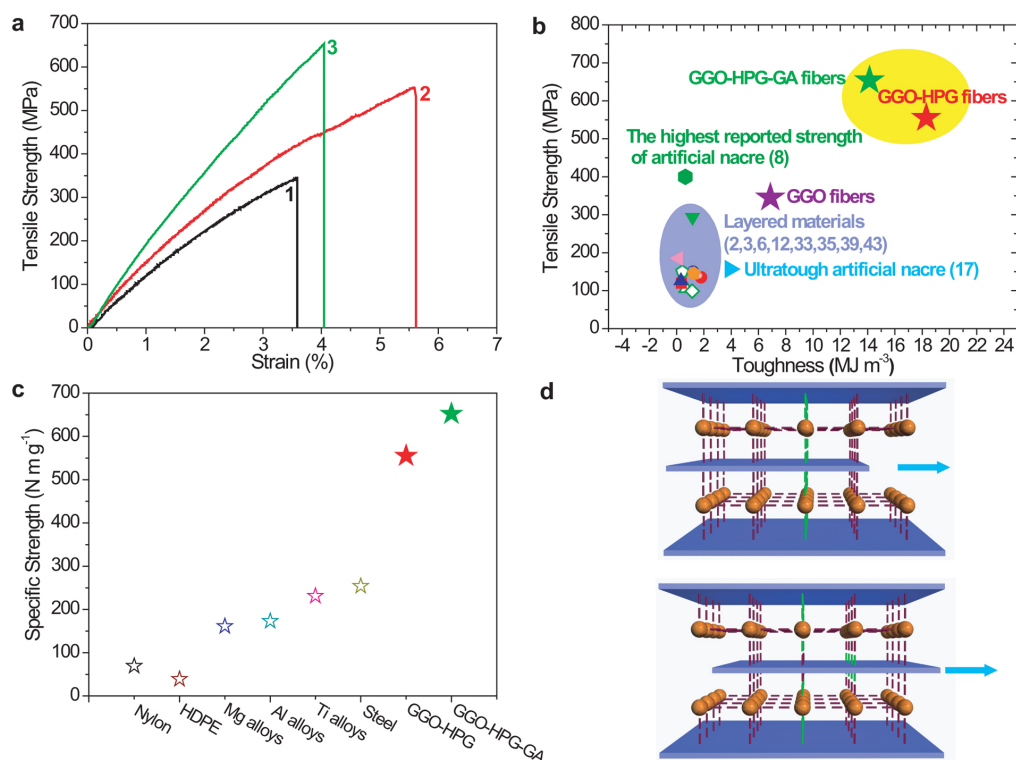


Figure 3 | Mechanical properties of fibres. (a) Typical stress-strain curves for neat GGO (1), GGO-HPG (2), and GGO-HPG-GA (3) fibres. The strain rate is 10% per minute. (b) Comparison of our bio-mimetic composites with nacre, bone, and reported layer-structured nanocomposites in terms of σ and volumetric toughness. (c) Comparison of our bio-mimetic composites with typical metallic alloys and engineering plastics in terms of specific strength. (d) Schematic illustration of the adaptive hydrogen bonding networks in GGO-HPG composites. The hydrogen bondings (marked in green) are destructed under tension and reformed subsequently as graphene sheets slip (shown in the below scheme).

Mechanical properties of GGO-HPG-GA fibres. In order to further improve the mechanical performance of GGO-HPG fibres, the interactions between HPG molecules and GGO should be enhanced. Therefore, our fibres were treated with GA to construct covalent acetal bridges between -OH groups of HPG and GGO. The resulting GGO-HPG-GA fibres remained layered structures (Supplementary Fig. S9), and further improved σ by 17.5% up to 652 MPa (Fig. 3a). This value approaches 38% of theoretical strength of GO-PVA composites (~ 1.7 GPa)³⁶. In addition, the Young's modulus (E) of GGO-HPG-GA fibres is 20.9 GPa, which is close to the theoretical E of GO-PVA composites (26 GPa)³⁶. Interestingly, the cross-linked fibres still keep comparable ϵ (4.1%) and toughness (14 MJ m^{-3}), offering a new model for nanocomposites to exceed natural materials.

The ultrastrong strength of our composites probably originates from the regular alignment of GGO sheets along the fibre axis, the waviness of GGO sheets in fibres, and the uniform d -space between neighboring GGO sheets. The marriage of intrinsic ordering of LCs and wet-spinning technology enables macroscopically assembled

materials aligned structures (Fig. 2g–k). The flexibility of GGO sheets provides curves perpendicular to the GGO sheets during the spinning process, which contribute additional forces to the mechanical performance. LCST approach realized the precise control over HPG content of biomimetic composites and uniform d -space between GGO sheets. We have fabricated GGO-HPG composites with different fractions of HPG (15.8–30.7 wt%, Fig. 5a,b) with increasing d -space of 10.27–12.68 Å (Fig. 5c,d). At an optimum fraction (23.2 wt%, d -space of 11.51 Å) of HPG, the highest σ (555 MPa) of composites was achieved (Fig. 5b). Under such a fraction, HPG formed shoulder-to-shoulder single molecular interlayer between two neighboring GGO sheets, resulting in even d -space and less voids (and thus the strongest interaction of hydrogen bonding array). Either less or more HPG led to decrease of available hydrogen bondings between adjacent GGO sheets and lower mechanical strength of composites due to more voids and irregular interspaces (Fig. 5b, Supplementary Fig. S10).

Performance of reduced composites. Through thermal or chemical reduction, the as-prepared GGO-HPG fibres were reduced to RGG-

Table 1 | Mechanical Properties of Nacre and Typical Artificial Nacre Composites

Composites	Volume fraction of platelets (%)	Tensile Strength (MPa)	Relative strength	Toughness (MJ m^{-3})	Strain (%)	Young's modulus (GPa)
Nacre (3)	95	80–135	~ 3.3	0.2–1.8	0.1–1	60–70
MTM/cross linked PVA (8)	50	400	10	0.64	0.33	106
Al_2O_3 /chitosan (10)	15	315	6	37.57	21	9.6
GO-PVA (16)	41	162	2	2.55	3	10
GO-chitosan (15)	6	206	2.7	6.18	6.5	6.3
GGO-HPG	77	555	$\sim 10^3$	18	5.6	15.9
GGO-HPG-GA	77	652	$\sim 10^3$	14	4.0	20.9

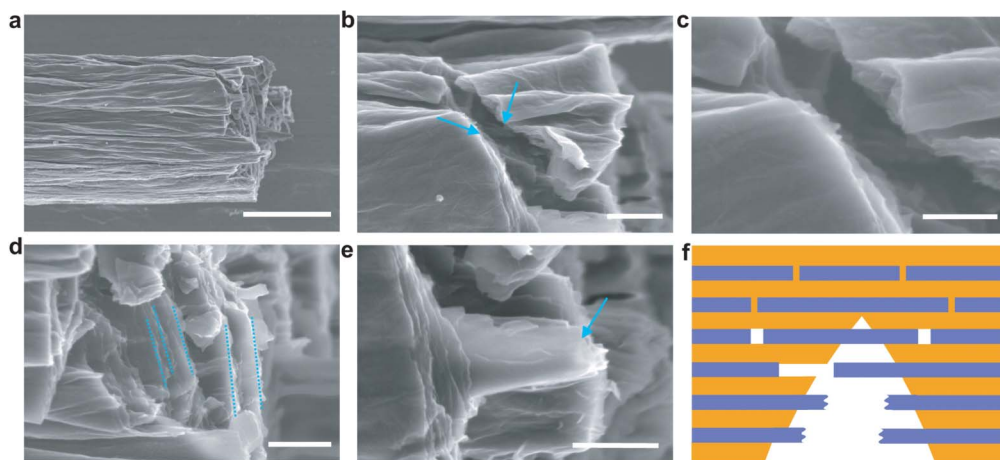


Figure 4 | Morphology of fracture section of GGO-HPG fibres. (a–e) SEM images of fracture surfaces of GGO-HPG fibres at different magnification. (f) Deformation mechanism model of GGO-HPG fibres under tensile stress. Scale bars, 5 μm (a) and 500 nm (b,d,e), 250 nm (c).

HPG fibres by removing the original oxygen containing groups on GGO sheets and restoration of conjugated nets. FT-IR spectrum of RGG-HPG indicates the oxygen moieties of GGO decreased obviously, thus the hydrogen bonding interactions should reduce (Supplementary Fig. S6). Raman spectra of GGO-HPG and RGG-HPG showed the restoration of conjugated nets. The characteristic peaks of graphene are the defect-induced D band at $\sim 1,355\text{ cm}^{-1}$, and G band at $\sim 1,595\text{ cm}^{-1}$ that is related to in-plane vibration of sp^2 carbon atoms in a 2D hexagonal lattice, respectively (Supplementary Fig. S11). The intensity ratio of D to G band (I_D/I_G) for GGO-HPG (~ 1.62), related to the size of the sp^2 domains, decreased

to ~ 1.25 for RGG-HPG, indicating the conjugated network of graphene recovered partially after reduction⁴⁵.

Here we chose several reducing agents, mainly including hydrazine monohydrate³⁹, environment-friendly vitamin C (Vc)⁴⁶, hydroiodic acid (HI)⁴⁷, and acetic acid (AcOH) to obtain RGG-HPG fibres⁴⁸. The corresponding electrical conductivities and mechanical properties were summarized in Table 2. The highest electrical conductivity of RGG-HPG composites, which was one order of magnitude higher than that of graphene/polyaniline composite films (550 S m^{-1})⁴⁹ and comparable to neat graphene papers ($\sim 6000\text{ S m}^{-1}$)³⁹, was achieved by reducing with HI-AcOH (5261 S m^{-1})

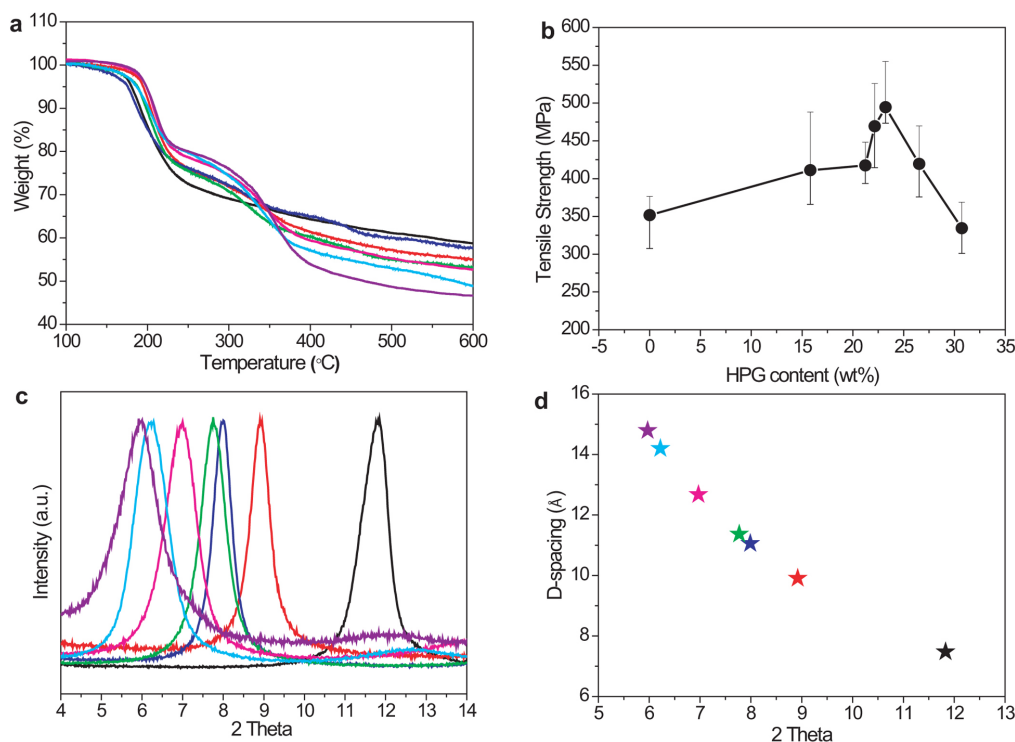


Figure 5 | Controlled structure of GGO-HPG composites. (a) TGA curves of neat GGO (black line) and GGO-HPG composites with different HPG fractions. (b) The σ of GGO-HPG composites as a function of HPG contents. (c) XRD patterns of neat GGO (black line) and GGO-HPG composites with different HPG contents. (d) The interlayer d -space of GGO-HPG composites as a function of 2 Theta. Error bars in b represent the minimum and maximum values obtained from eight independent experiments.



Table 2 | Electrical Conductivities and Mechanical Properties of RGG-HPG Fibres

Reducing Method	Electrical Conductivity ($S m^{-1}$)	Tensile Strength (MPa)	Strain (%)	Toughness ($MJ m^{-3}$)	Young's modulus (GPa)
$N_2H_4 \cdot H_2O$	244	42	2.6	0.6	2.5
Vc	1165	429	4.0	9.3	14.3
Modified Vc	2585	533	5.1	14.4	14.4
HI	3209	443	5.6	14.0	10.8
HI+AcOH	5261	487	3.5	9.5	17.6
200°C	41	487	5.9	15.3	10.8

(Fig. 6a, Supplementary Fig. S12). The corresponding RGG-HPG composites also showed good mechanical performance (σ 487 MPa, ϵ 3.5%, E 17.6 GPa, Fig. 6b). The composites reduced by hydrazine monohydrate had obvious porous structures (Supplementary Fig. S13), accordingly exhibiting much lower electrical conductivity ($244 S m^{-1}$) and the minimal mechanical strength (42 MPa). Furthermore, we developed an efficient and nontoxic reduction method with Vc and KOH as reducing agent, and the RGG-HPG fibres displayed an electrical conductivity of $2584 S m^{-1}$, two times that of composite reduced by the previous Vc protocol ($1164 S m^{-1}$)⁴⁶. Noticeably, our modified Vc approach provided the strongest σ and the best toughness (σ 533 MPa, ϵ 5.1%, E 14.4 GPa, toughness of $14.4 MJ m^{-3}$) among RGG-HPG composites made by the different reducing methods. The strength of RGG-HPG composites was mostly comparable to those of original GGO-HPG fibres, mainly because of the highly ordered hierarchical structures of composites. Recently, Buehler and coworkers also theoretically demonstrated that the mechanical performance of bio-mimetic composites was majorly dependent on their hierarchical structures rather than constituents^{50,51}. The high conductivities together with their ultrastrong and tough properties make our bio-mimetic fibres widely applicable in the fields of multifunctional textiles and wearable electronic devices⁵².

Versatility of LCST Strategy. To confirm the versatility of our LCST strategy, linear polymer guests such as PVA were utilized to mix with the host of GGO LCs, and continuous strong fibres were also obtained by the same wet-spinning assembly protocol (Supplementary Fig. S14). Additionally, Ag nanoparticles were synthesized utilizing HPG as stabilizer⁵³, and layer-structured GGO-HPG-Ag fibres were also obtained via the LCST approach. X-ray energy dispersive analysis proved the uniform distribution of Ag element in the cross-section of the fibres (Supplementary Fig. S15).

Discussion

Compared with previous artificial nacre composites, GGO-HPG fibres show great enhancement in both σ and ϵ , mainly because

the chosen GGO building blocks have extraordinary properties that can be translated into the macroscopic GGO-HPG fibres by effective assembly. The large size of GGO minimizes the defects in our composites. The combination of LCST strategy and wet-spinning process provides effective assembly and ordered alignment of building blocks. The flexible feature of GGO generates wrinkles and waviness during the spinning process, which are favorable to improve the strength. The formation of strong and adaptive hydrogen bonding networks between GGO and HPG also contributes to the super properties. As the adaptive character of hydrogen bonding network, the destructed hydrogen bondings can be recovered for a number of cycles, providing our composites good ductility⁵⁴. Moreover, the uniform monolayer of HPG molecules maximizes the quantity of hydrogen bondings, which can repair some defects and further improve the mechanical strength of our composites.

For the neat GGO system, three kinds of dominant interactions between individual GGO sheets, van der Waals interactions, hydrogen bondings, and ionic interactions (Supplementary Fig. S16), contribute to its mechanical strength (σ 345 MPa). Considering that hydrogen bondings need oxygen containing groups, HPG with abundant hydroxyl groups were introduced to increase the density of hydrogen bondings at both interlayer and intralayer (Supplementary Fig. S6), further improving σ to 555 MPa. The supramolecular interactions were successfully converted into stronger covalent linkages by cross-linking with GA, resulting in higher mechanical properties (σ 652 MPa, E 20.9 GPa).

After chemical reduction, the RGG-HPG composites mostly maintained good performance from the original GGO-HPG fibres (Table 2) due to the increased van der Waals interactions between graphene sheets (Supplementary Fig. S11), slightly decreased hydrogen bondings and ionic interactions (Supplementary Fig. S6), as well as the hierarchical structure of composites. In GGO-HPG composites, the large size and waviness of GGO sheets and the dendritic binder structure of HPG give the primary structure of fibres; the high density of hydrogen bondings between HPG and GGO provide the secondary structure; the regular and compact cross-section derived from the LC structures of GGO-HPG aqueous solution and effective

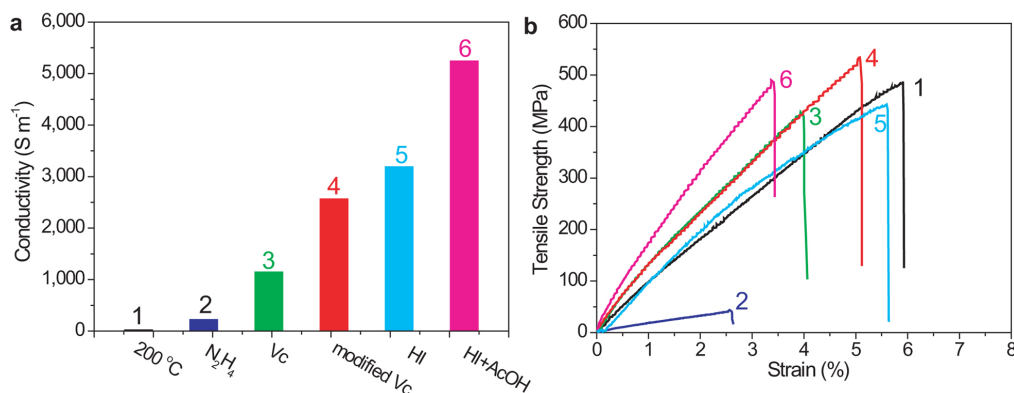


Figure 6 | Properties of RGG-HPG fibres. (a) Electrical conductivities of RGG-HPG fibres reduced by different methods. (b) Typical stress-strain curves of RGG-HPG composites, reduced by 200°C thermal treatment (1), N_2H_4 (2), Vc (3), modified Vc (4), HI (5), and HI+AcOH (6).



assembly by wet-spinning form the tertiary structure; the alignment and wrinkles (formed in the coagulation procedure) of GGO sheets along the fibre axis make up the quarternary structure. These four hierarchical levels of GGO-HPG fibres not only provide high strength and toughness of original composites, but also are responsible for the comparable mechanical performance of RGG-HPG composites since such hierarchical structures remained after reduction.

Although most of RGG-HPG fibres obtained by different methods remain excellent properties, the stress-strain curves are distinct. Thermal treatment reserved compact cross-section structure of GGO-HPG (Supplementary Fig. S13), resulting in comparable mechanical performance. The chemical reduction of GGO-HPG fibres may create new products and change the compositions of RGG-HPG fibres, which differ from each other according to the reducing agents^{46–48}, thus the stress-strain curves are sensitive to the reduction methods. Notably, the hydrazine reduction process may generate gas, which results in porous structure of RGG-HPG fibres (Supplementary Fig. S13), seriously decreasing the mechanical properties.

A typical shear lag model has been proposed to illustrate the strength of nacre. Based on this model, two fracture types of layered composites are found, according to the aspect ratio (S) of platelets and the critical one (S_c). Generally, S_c is equal to the ratio of tensile strength of platelets (σ_p) and shear strength of organic matrix (τ_y) ($S_c = \sigma_p/\tau_y$). For $S < S_c$, the relatively weak organic matrix and the interface of platelet-organic matrix yield the tensile strength, and thus the composites break by pull-out of platelets. In the case of $S > S_c$, the composites fail due to the fracture of platelets. The later case usually gives stronger but brittle materials. In our composites, S_c is around 10^4 , close to the aspect ratio of part GGO sheets ($S \sim 1.6 \times 10^4$). Therefore, we observed the fracture of GGO sheets in GGO-HPG composites (Fig. 4b,c). As the GGO sheets have a wide distribution of width, some GGO platelets pulled out accompanying the rupture of composites (Fig. 4d,e). Moreover, the incorporation of adaptive hydrogen bondings between GGO and HPG further provided the composites ductile attribute, resulting in high ϵ and toughness.

In summary, we designed a green, simple, general, fast and efficient LCST strategy to fabricate the next generation of continuous, ultrastrong and tough bio-mimetic composites. Despite of the mechanical blending process, phase separation between nanofillers and polymer was avoided, even at the case of high content of nanoparticles (~ 77 wt%). The uniform, regular arrangement and the high aspect ratio of GGO sheets together with the hierarchical structures of our composites led to a large improvement of mechanical performance for nanocomposites. The biomimetic composites set a new record σ (~ 0.65 GPa) and toughness (~ 18 MJ m⁻³) among nacre mimics. In addition, the composites exhibited high electrical conductivity (5261 S m⁻¹) that was comparable to neat graphene papers. Such multifunctional composites have wide applications in functional textiles as well as flexible and wearable devices. The LCST strategy can be readily extended to prepare other hierarchically structured composites that can be hardly accessed by previous protocols, opening the avenue to multifunctional, highly ordered and tailor-made materials.

Methods

Preparation of GGO-HPG fibres. Given amount of HPG was added to GGO LCs, and the mixture was stirred sufficiently for 24 h at room temperature. The GGO-HPG LCs (5–8 mg mL⁻¹) were loaded into a plastic syringe with a spinning nozzle (PEK tube with diameter of 100 μ m) and injected into 5 wt% CaCl₂ solution by an injection pump (20 μ L min⁻¹). After coagulation for 15 minutes, the fibres were rinsed by water for two times, rolled onto the drum, and dried for 24 h under 60 °C in vacuum, giving rise to the final products.

Preparation of GGO-HPG-GA fibres. The as-prepared GGO-HPG fibres were immersed in glutaraldehyde (25%) for a week at room temperature. After being dried for 24 h under 80 °C in vacuum, GGO-HPG-GA fibres were obtained.

Instruments. SEM images were obtained on a Hitachi S4800 field-emission SEM system. POM observations were performed with a Nikon E600POL and the liquid samples were loaded into the planar cells for observations. The tensile stress-strain tests were performed on a Microcomputer Control Electronic Universal Testing Machine made by REGER in China (RGWT-4000-5). The strain rate is 10% per minute. Thermal gravimetric analysis (TGA) was carried out on a Perkin-Elmer Pyris 6 TGA instrument with a heating rate of 20 °C min⁻¹ under a nitrogen flow (30 mL min⁻¹). XRD data were collected with an X'Pert Pro (PANalytical) diffractometer using monochromatic Cu K α 1 radiation ($\lambda = 1.5406$ Å) at 40 kV. Fourier-transform infrared (FTIR) spectra were recorded on a Bruker Vector 22 spectrometer. TEM analysis was performed on a JEOL JEM1200EX electron microscope at 120 KV. Electrical properties were measured on CHI660E workstation.

- Ritchie, R. O. The conflicts between strength and toughness. *Nat. Mater.* **10**, 817–822 (2011).
- Yao, H. B., Fang, H. Y., Wang, X. H. & Yu, S. H. Hierarchical assembly of micro-/nano-building blocks: bio-inspired rigid structural functional materials. *Chem. Soc. Rev.* **40**, 3764–3785 (2011).
- Wang, J. F., Cheng, Q. F. & Tang, Z. Y. Layered nanocomposites inspired by the structure and mechanical properties of nacre. *Chem. Soc. Rev.* **41**, 1111–1129 (2012).
- Grégoire, C. Topography of the organic components in mother-of-pearl. *J. Biophysic. Biochem. Cytol.* **3**, 797–808 (1957).
- Clegg, W. J., Kendall, K., Alford, N. M., Button, T. W. & Birchall, J. D. A simple way to make tough ceramics. *Nature* **347**, 455–457 (1990).
- Tang, Z. Y., Kotov, N. A., Magonov, S. & Ozturk, B. Nanostructured artificial nacre. *Nat. Mater.* **2**, 413–418 (2003).
- Deville, S., Saiz, E., Nalla, R. K. & Tomsia, A. P. Freezing as a path to build complex composites. *Science* **311**, 515–518 (2006).
- Podsiadlo, P. *et al.* Ultrastrong and stiff layered polymer nanocomposites. *Science* **318**, 80–83 (2007).
- Munch, E. *et al.* Tough, Bio-inspired hybrid materials. *Science* **322**, 1516–1520 (2008).
- Bonderer, L. J., Studart, A. R. & Gauckler, L. J. Bioinspired design and assembly of platelet reinforced polymer films. *Science* **319**, 1069–1073 (2008).
- Walther, A. *et al.* Large-area, lightweight and thick biomimetic composites with superior material properties via fast, economic, and green pathways. *Nano. Lett.* **10**, 2742–2748 (2010).
- Yao, H. B., Fang, H. Y., Tan, Z. H., Wu, L. H. & Yu, S. H. Biologically inspired, strong, transparent, and functional layered organic-inorganic hybrid films. *Angew. Chem. Int. Ed.* **49**, 2140–2145 (2010).
- Walther, A. *et al.* Supramolecular control of stiffness and strength in lightweight high-performance nacre-mimetic paper with fire-shielding properties. *Angew. Chem. Int. Ed.* **49**, 6448–6453 (2010).
- Yao, H. B., Tan, Z. H., Fang, H. Y. & Yu, S. H. Artificial nacre-like bionanocomposite films from the self-assembly of chitosan-montmorillonite hybrid building blocks. *Angew. Chem. Int. Ed.* **49**, 10127–10131 (2010).
- Wang, X. L., Bai, H., Yao, Z. Y., Liu, A. R. & Shi, G. Q. Electrically conductive and mechanically strong biomimetic chitosan/reduced graphene oxide composite films. *J. Mater. Chem.* **20**, 9032–9036 (2010).
- Li, Y. Q., Yu, T., Yang, T. Y., Zheng, L. X. & Liao, K. Bio-inspired nacre-like composite films based on graphene with superior mechanical, electrical, and biocompatible properties. *Adv. Mater.* **24**, 3426–3431 (2012).
- Cheng, Q. F., Wu, M. X., Li, M. Z., Jiang, L. & Tang, Z. Y. Ultratough artificial nacre based on conjugated cross-linked graphene oxide. *Angew. Chem. Int. Ed.* **52**, 3750–3755 (2013).
- Bisoyi, H. K. & Kumar, S. Liquid-crystal nanoscience: an emerging avenue of soft self-assembly. *Chem. Soc. Rev.* **40**, 306–319 (2011).
- Shopsowitz, K. E., Qi, H., Hamad, W. Y. & MacLachlan, M. J. Free-standing mesoporous silica films with tunable chiral nematic structures. *Nature* **468**, 422–425 (2010).
- Chung, W. J. *et al.* Biomimetic self-templating supramolecular structures. *Nature* **478**, 364–368 (2011).
- Song, W. H., Kinloch, I. A. & Windle, A. H. Nematic liquid crystallinity of multiwall carbon nanotubes. *Science* **302**, 1363 (2003).
- Song, W. H. & Windle, A. H. Size-dependence and elasticity of liquid-crystalline multiwalled carbon nanotubes. *Adv. Mater.* **20**, 3149–3154 (2008).
- Vigolo, B. *et al.* Macroscopic fibres and ribbons of oriented carbon nanotubes. *Science* **290**, 1331–1334 (2000).
- Davis, V. A. *et al.* True solutions of single-walled carbon nanotubes for assembly into macroscopic materials. *Nat. Nanotechnol.* **4**, 830–834 (2009).
- Geim, K. Graphene: Status and prospects. *Science* **324**, 1530–1534 (2009).
- Xu, Z. & Gao, C. Aqueous liquid crystals of graphene oxide. *ACS Nano* **5**, 2908–2915 (2011).
- Kim, J. E. *et al.* Graphene oxide liquid crystals. *Angew. Chem. Int. Ed.* **50**, 3043–3047 (2011).
- Behabtu, N. *et al.* Spontaneous high-concentration dispersions and liquid crystals of graphene. *Nat. Nanotech.* **5**, 406–411 (2010).
- Xu, Z. & Gao, C. Graphene chiral liquid crystals and macroscopic assembled fibres. *Nat. Commun.* **2**, 571 (2011).



30. Xu, Z., Sun, H. Y., Zhao, X. L. & Gao, C. Ultrastrong fibres assembled from giant graphene oxide sheets. *Adv. Mater.* **25**, 188–193 (2013).
31. Dong, Z. L. *et al.* Facile fabrication of light, flexible and multifunctional graphene fibres. *Adv. Mater.* **24**, 1856–1861 (2012).
32. Xu, Z., Zhang, Y., Li, P. G. & Gao, C. Strong, conductive, lightweight, neat graphene aerogel fibres with aligned pores. *ACS Nano* **6**, 7103–7113 (2012).
33. Hu, X. Z., Xu, Z. & Gao, C. Multifunctional, supramolecular, continuous artificial nacre fibres. *Sci. Rep.* **2**, 767 (2012).
34. Kou, L. & Gao, C. Bioinspired design and macroscopic assembly of poly(vinyl alcohol)-coated graphene into kilometers-long fibres. *Nanoscale* **5**, 4370–4378 (2013).
35. An, Z., Compton, O. C., Putz, K. W., Brinson, L. C. & Nguyen, S. T. Bio-inspired borate cross-linking in ultra-stiff graphene oxide thin films. *Adv. Mater.* **23**, 3842–3846 (2011).
36. Compton, O. C. *et al.* Tuning the mechanical properties of graphene oxide paper and its associated polymer nanocomposites by controlling cooperative intersheet hydrogen bonding. *ACS Nano* **6**, 2008–2019 (2012).
37. Chae, H. G. & Kumar, S. Making strong fibres. *Science* **319**, 908 (2008).
38. Wegst, U. G. K. & Ashby, M. F. The mechanical efficiency of natural materials. *Philos. Mag.* **84**, 2167–2181 (2004).
39. Chen, H. Q., Müller, M. B., Gilmore, K. J., Wallace, G. G. & Li, D. Mechanically strong, electrically conductive, and biocompatible graphene paper. *Adv. Mater.* **20**, 3557–3561 (2008).
40. Rho, J. Y., Spearing, L. K. & Zioupos, P. Mechanical properties and the hierarchical structure of bone. *Med. Eng. Phys.* **20**, 92–102 (1998).
41. Wang, R. Z., Suo, Z., Evans, A. G., Yao, N. & Aksay, I. A. Deformation mechanisms in nacre. *J. Mater. Res.* **16**, 2485–2493 (2001).
42. Tan, Y. Q., Song, Y. H. & Zheng, Q. Hydrogen bonding-driven rheological modulation of chemically reduced graphene oxide/poly(vinyl alcohol) suspensions and its application in electrospinning. *Nanoscale* **4**, 6997–7005 (2012).
43. Park, S. J. *et al.* Graphene oxide papers modified by divalent ions-enhancing mechanical properties via chemical cross-linking. *ACS Nano* **2**, 572–578 (2008).
44. Shin, M. K. *et al.* Synergistic Toughening of Composite Fibres by Self-Alignment of Reduced Graphene Oxide and Carbon Nanotubes. *Nat. Commun.* **3**, 650 (2012).
45. He, H. K. & Gao, C. General approach to individually dispersed, highly soluble, and conductive graphene nanosheets functionalized by nitrene chemistry. *Chem. Mater.* **22**, 5054–5064 (2010).
46. Gao, J. *et al.* Environment-friendly method to produce graphene that employs vitamin C and amino acid. *Chem. Mater.* **22**, 2213–2218 (2010).
47. Pei, S. F., Zhao, J. P., Du, J. H., Ren, W. C. & Cheng, H. M. Direct reduction of graphene oxide films into highly conductive and flexible graphene films by hydrohalic acids. *Carbon* **48**, 4466–4474 (2010).
48. Moon, I. K., Lee, J., Ruoff, R. S. & Lee, H. Reduced graphene oxide by chemical graphitization. *Nat. Commun.* **1**, 73 (2010).
49. Wu, Q., Xu, Y. X., Yao, Z. Y., Liu, A. R. & Shi, G. Q. Supercapacitors based on flexible graphene/polyaniline nanofibre composite films. *ACS Nano* **4**, 1963–1970 (2010).
50. Buehler, M. J. Tu(r)ning weakness to strength. *Nano Today* **5**, 379–383 (2010).
51. Sen, D. & Buehler, M. J. Structural hierarchies define toughness and defect-tolerance despite simple and mechanically inferior brittle building blocks. *Sci. Rep.* **1**, 35 (2011).
52. Gao, Y. & Tang, Z. Y. Design and application of inorganic nanoparticle superstructures: current status and future challenges. *Small* **7**, 2133–2146 (2011).
53. Zhou, L., Gao, C., Hu, X. Z. & Xu, W. J. General avenue to multifunctional aqueous nanocrystals stabilized by hyperbranched polyglycerol. *Chem. Mater.* **23**, 1461–1470 (2011).
54. Qin, B. *et al.* Reversible photoswitchable fluorescence in thin films of inorganic nanoparticle and polyoxometalate assemblies. *J. Am. Chem. Soc.* **132**, 2886–2888 (2010).

Acknowledgments

This work was supported by the National Natural Science Foundation of China (No. 51173162), Qianjiang Talent Foundation of Zhejiang Province (No. 2010R10021), Fundamental Research Funds for the Central Universities (No. 2013XZZX003), and Research Fund for the Doctoral Program of Higher Education of China (No. 20100101110049) and Zhejiang Provincial Natural Science Foundation of China (No. R4110175). We thank the staffs of BL16B1 Beamline in the Shanghai Synchrotron Radiation Facility and the key project (Z12sr0042) for SAXS characterizations.

Author contributions

C.G. conceived the concept, X.Z.H. and C.G. designed the research, analysed the experimental data and wrote the paper; X.Z.H. conducted the experiments; Z.X. and Z.L. joined the discussion of data and gave some useful suggestions; C.G. supervised and directed the project.

Additional information

Supplementary information accompanies this paper at <http://www.nature.com/scientificreports>

Competing financial interests: The authors declare no competing financial interests.

How to cite this article: Hu, X.Z., Xu, Z., Liu, Z. & Gao, C. Liquid crystal self-templating approach to ultrastrong and tough biomimic composites. *Sci. Rep.* **3**, 2374; DOI:10.1038/srep02374 (2013).



This work is licensed under a Creative Commons Attribution-NonCommercial-NoDerivs 3.0 Unported license. To view a copy of this license, visit <http://creativecommons.org/licenses/by-nc-nd/3.0>